

Chlorine-Doped ZnSe Nanoribbons with Tunable n-Type Conductivity as High-Gain and Flexible Blue/UV Photodetectors

Zhi Wang,^[a] Jiansheng Jie,^{*[b]} Fangze Li,^[a] Li Wang,^[a] Tianxin Yan,^[a] Linbao Luo,^[a] Biao Nie,^[a] Chao Xie,^[a] Peng Jiang,^[a] Xiwei Zhang,^[b] Yongqiang Yu,^[a] and Chunyan Wu^[a]

Although significant progress has been achieved in the fabrication of ZnSe nanostructures with various structures and morphologies, it remains a major challenge to rationally tune their transport properties for applications in future nano-optoelectronic devices. The synthesis of chlorine-doped ZnSe nanoribbons (NRs) with tunable n-type conductivity is achieved by a thermal co-evaporation method. The ZnSe:Cl NRs have single-crystal wurtzite structure and [120] orientation, which also show high crystalline quality and structural integrity comparable with the undoped NRs. Electrical measurements on a single ZnSe:Cl NR reveal a substantial enhancement of the

conductivity upon Cl doping. The conductivity could be further tuned by adjusting the doping level. In addition, highly sensitive blue/UV photodetectors are constructed based on the ZnSe:Cl NRs. The devices exhibit an extremely high gain of approximately 10^6 , and the UV response could be enhanced through a fast annealing process in air. By replacing the rigid SiO₂/Si substrate with a PET substrate, flexible ZnSe:Cl NR photodetectors with excellent stability and durability under strain are realized. It is expected that the ZnSe:Cl NRs with tunable n-type conductivity will have important applications in the new generation nano-optoelectronic devices.

Introduction

Semiconductor nanostructures with exceptional properties have emerged as important building blocks for next-generation nanoelectronics and nano-optoelectronics. To promote their device applications, however, the capability to rationally tune their electronic and optoelectronic properties is essential. The doping technique is regarded as one of the most efficient methods for this purpose owing to its versatile use of different functionalities. Optical, magnetic, electronic, and optoelectronic properties of the nanostructures could be remarkably enhanced and finely tuned by introducing appropriate foreign elements into them. Thereby tremendous efforts have been devoted to implement doping in nanostructures. The successful realization of complementary doping, i.e. both n- and p-type doping, in IV and III–V group nanostructures has led to the actualization of a variety of novel nanodevices, such as complementary metal-oxide-semiconductor transistors (CMOS),^[1] light-emitting diodes (LEDs),^[2] laser diodes (LDs),^[3] photovoltaic devices,^[4] and so on. In spite of this progress, studies on the controlled doping of the semiconductor nanostructures, particularly in II–VI group nanostructures, are critical and still at their very initial stages.

ZnSe is an important II–VI group semiconductor with a wide direct band-gap of approximately 2.7 eV at room temperature. It has been widely used in LEDs, LDs, and photodetectors operated in the blue to ultraviolet (UV) range. In the past decade, synthesis of ZnSe nanostructures has been intensively studied and various growth methods have been developed to obtain ZnSe nanowires (NWs) and nanoribbons (NRs).^[5–7] Although Mn, Ag, and Cu doping have been utilized to modulate their optical and structural properties,^[8–10] n- and p-type doping in

ZnSe nanostructures have been rarely investigated and remain a challenge. As we known, p-type doping in II–VI group films is often obstructed by the serious self-compensation effect,^[11] that is, the acceptors introduced into the II–VI group films are usually counteracted by the generation of more donor defects. In contrast, we recently demonstrated efficient p-type doping in ZnSe NWs and ZnS NRs with a high hole concentration by using V group elements such as Bi and Sb as the dopants.^[12,13] The high crystalline quality and consequently less intrinsic defects are likely responsible for the superior p-type doping behavior of the II–VI group nanostructures. This progress may open new opportunities for the nano-optoelectronic applications of the II–VI group nanostructures by constructing the homojunctions based on them, while only heterojunctions such as n-CdS NW/p-Si have been studied so far.^[14] Considering that both p- and n-type doping are demanded for constituting the homojunctions, achieving efficient n-type doping in II–VI group nanostructures is urgently required.

Herein, we describe the synthesis of n-type ZnSe NRs by using ZnCl₂ as the Cl dopant through a thermal co-evaporation method. The conductivity of the ZnSe NRs was remarkably en-

[a] Z. Wang, F. Z. Li, Prof. L. Wang, T. X. Yan, Prof. L. B. Luo, B. Nie, C. Xie, P. Jiang, Y. Q. Yu, Prof. C. Y. Wu
School of Electronic Science and Applied Physics
Hefei University of Technology
Hefei Anhui 230009 (P. R. China)

[b] Prof. J. S. Jie, X. W. Zhang
Institute of Functional Nano & Soft Materials (FUNSOM)
Jiangsu Key Laboratory for Carbon-Based Functional Materials & Devices
Soochow University, Suzhou Jiangsu 215123 (P. R. China)

hanced upon doping and could be tuned up to three orders of magnitude by adjusting the doping level. The doped NRs exhibited great potential as blue/UV light photodetectors with extremely high photoconductive gain. Their application in flexible optoelectronics was further exploited by using polyethylene terephthalate (PET) as the device substrates.

Results and Discussion

Figure 1a shows a typical SEM image of the ZnSe:Cl NRs, indicating that the NRs have width in the range of 500 nm–3 μ m, length of 30–100 μ m, and thickness of 10–60 nm. It is noted that the ZnSe:Cl NRs are uniform along the length with clean

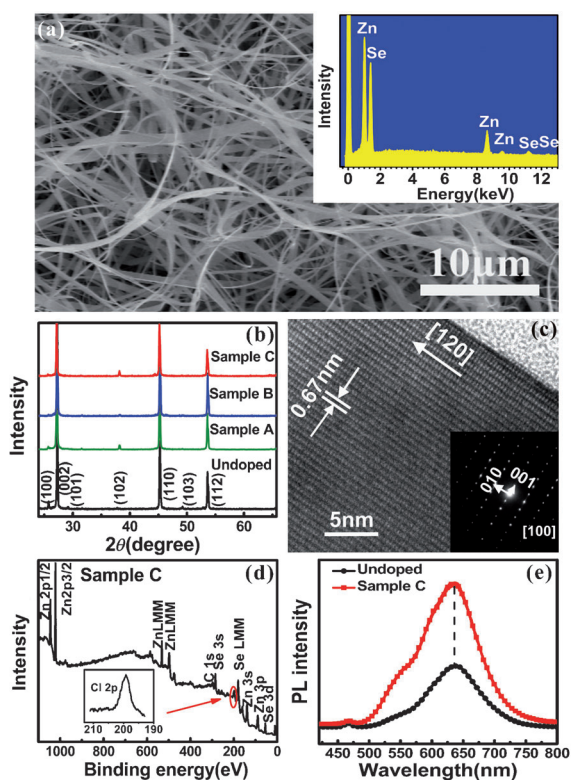


Figure 1. a) Typical FESEM image of the as-synthesized chlorine-doped ZnSe NRs. Inset shows the corresponding EDS spectrum. b) The XRD patterns of both the undoped and doped ZnSe NRs. c) HRTEM image of the ZnSe:Cl NR. Inset shows the corresponding SAED pattern. d) The XPS spectrum of ZnSe:Cl NRs (Sample C). Inset shows the enlarged Cl 2p peak centered at approximately 199.2 eV. e) The PL spectra of both the undoped and doped (Sample C) ZnSe NRs.

and smooth surfaces and free of visible particles and impurities. From the energy-dispersive X-ray spectroscopy (EDS) profile of Sample C (inset in Figure 1a), the Zn/Se atomic ratio is estimated to be about 48:52, which is close to the stoichiometric ratio of ZnSe. The X-ray diffraction (XRD) patterns of the ZnSe:Cl NRs, together with the undoped sample for comparison, are shown in Figure 1b. All the diffraction peaks in the patterns could be properly assigned to ZnSe with a wurtzite structure (JCPDS no. 80-0008),^[15] and no obvious peak shift is observed for the doped samples, which might be attributed to

the similar ionic radius of Cl⁻ (1.81 Å) with Se²⁻ (1.91 Å). The typical high-resolution transmission electron microscopy (HRTEM) image and corresponding selected-area electron diffraction (SAED) pattern of the ZnSe:Cl NR are shown in Figure 1c. The (001) and (010) planes with lattice space of 0.67 nm and 0.34 nm, respectively, could be clearly distinguished in the HRTEM image, thus revealing that the NRs are single crystalline with wurtzite structure and [120] growth orientation. The NR shows atomically sharp edge without any amorphous outer layer, which is clear evidence of the high quality of the ZnSe:Cl NRs.

Figure 1d shows the X-ray photoelectron spectroscopy (XPS) spectrum of the ZnSe:Cl NRs (Sample C). In addition to the peaks corresponding to Zn and Se, a weak peak at approximately 199.0 eV that corresponds to the Cl 2p core level emission is observed, thus indicating the existence of the element Cl in the sample. The content of Cl is estimated to be approximately 2% from the XPS spectrum. In contrast, no Cl signal could be detected in the undoped sample, thus implying that efficient Cl doping has been achieved in the ZnSe NRs. Figure 1e shows the photoluminescence (PL) spectra of both the doped and undoped ZnSe NRs. The PL peaks at 460 nm (2.73 eV) can be ascribed to the near-band edge (NBE) emission of ZnSe,^[16] whereas the peaks at around 630 nm are associated with the deep-level emissions, which are assigned as donor-to-acceptor pair (DAP) transitions related to self-activated (SA) zinc vacancies.^[17–19] Note that the deep-level emission becomes stronger upon Cl doping, which is a result of the increased Cl_{Se}-V_{Zn} concentration. The peak position and width of the doped sample are near identical to the undoped one except the change in band intensity, thus revealing that the crystalline quality and structural integrity of the ZnSe NRs are not seriously degraded by the incorporation of Cl. This feature will be conducive to the optoelectronic applications of the ZnSe:Cl NRs.

To assess the effect of Cl doping on the transport properties of the NRs, field-effect transistors (FETs) were constructed based on the individual ZnSe:Cl NRs (Figure 2a). Figure 2b plots the typical source–drain current (I_{DS}) versus source–drain voltage (V_{DS}) curves measured on the ZnSe:Cl NRs with varied doping level in the dark at zero gate bias. The good Ohmic contact of indium tin oxide (ITO) with the NRs was proven by the good linearity of the curves. It is noted that the use of ITO electrodes is vital to obtain this Ohmic contact, which could be interpreted by the formation of a highly conductive interfacial oxide layer between ITO and the ZnSe:Cl NRs, as a result, the surface Fermi level pinning of the NRs is eliminated giving a more efficient carrier injection from ITO to the NRs. Notably, the conductance of the ZnSe NRs increases remarkably with increasing the level of Cl doping. The undoped ZnSe NRs are highly insulating with conductance lower than 0.03 pS, while the chlorine-doped ZnSe NRs exhibit much improved conductance of 0.8 nS, 61 nS, and 1.4 μ S for Sample A, Sample B, and Sample C, respectively. To gain a statistical significance, the conductivities of 20 NRs were measured for each sample, and the corresponding conductivity distribution is shown in Figure 2c. As compared with the undoped NRs ($\approx 10^{-7}$ Scm⁻¹),

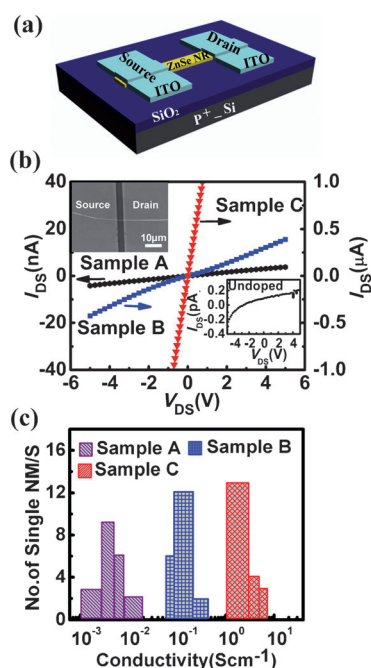


Figure 2. a) Schematic illustration of the back-gate FET based on a single ZnSe:Cl NR. b) Representative I - V curves of the ZnSe:Cl NRs with varied doping levels. I - V curve of the undoped ZnSe NR is shown in the right inset for comparison. Left inset shows the typical SEM image of the NR device. c) Conductivity distribution of the ZnSe:Cl NRs with different doping level, 20 devices each for Sample A, Sample B, and Sample C.

the conductivity of the ZnSe:Cl NRs has been dramatically enhanced with a maximum improvement of near eight order of magnitude for Sample C ($1\text{--}10\text{ Scm}^{-1}$). From Figure 2c, it is also clear that conductivity of the ZnSe:Cl NRs could be tuned in a wide range of about three orders of magnitude by adjusting the level of Cl doping.

Figure 3 shows the representative I_{DS} - V_{DS} curves of the ZnSe:Cl NRs measured at varied gate voltage (V_{GS}) ranging from -30 to $+30$ V in steps of $+10$ V, along with the I_{DS} - V_{GS} curves at fixed V_{DS} of $+1$ V. We note that all the devices exhibit an obvious gating effect and the conductance of the ZnSe:Cl NRs consistently increases with the increasing of V_{GS} . This feature is in good agreement with the typical characteristic of an n-channel metal-oxide semiconductor FET (MOSFET) and reveals the n-type nature of the ZnSe:Cl NRs. The n-type conductivity of the NRs could be attributed to the substitution of Se^{2-} ions by Cl^- ions in the ZnSe NRs. Table 1 summarizes the key parameters of the ZnSe:Cl NR FETs at various doping levels. It is seen that the I_{ON}/I_{OFF} ratio estimated from the I_{DS} at

ZnSe:Cl NRs	I_{ON}/I_{OFF}	V_{th} [V]	μ_n [$\text{cm}^2\text{V}^{-1}\text{s}^{-1}$]	σ [Scm^{-1}]	n [cm^{-3}]
Sample A	$\approx 10^3$	12.6	0.4	1.1×10^{-3}	1.8×10^{16}
Sample B	$\approx 10^2$	6.8	2.8	8.5×10^{-2}	1.9×10^{17}
Sample C	$\approx 10^1$	0.1	17.3	2.1	6.9×10^{17}

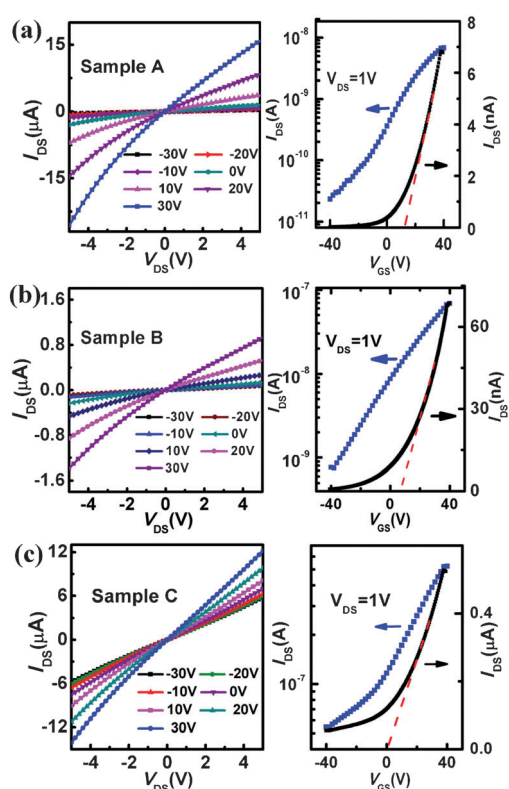


Figure 3. Electron-transfer characteristics of the back-gate FETs based on ZnSe:Cl NRs with different doping level. The I_{DS} - V_{DS} curves were measured under varied V_{GS} values ranging from -30 to $+30$ V with a voltage step of $+10$ V. The I_{DS} - V_{GS} curves were measured at fixed $V_{DS} = +1$ V. Parts (a), (b), and (c) corresponds to Sample A, Sample B, and Sample C, respectively.

the accumulation state ($+40$ V) and depletion state (-40 V) of the FETs has decreased from approximately 10^3 for Sample A to about 10^1 for Sample C. This outcome is a result of the increased carrier concentration and consequently weaker gate modulation to the conduction channel. Also, V_{th} , which is deduced by extracting the linear portion of the I_{DS} - V_{GS} curve, has decreased gradually from Sample A to C because lower voltage is needed to turn-on the devices at higher doping levels. The electron mobility (μ_n) can be estimated from the channel transconductance (g_m) of the ZnSe:Cl NR FETs in the linear regimes of the I_{DS} - V_{GS} curves. The g_m value is given by Equation (1):

$$g_m = \frac{dI_{DS}}{dV_G} = \left(\frac{Z}{L}\right)\mu_n C_0 V_{DS} \quad (1)$$

where Z/L is the ratio of channel width to channel length, C_0 ($1.15 \times 10^{-8}\text{ Fcm}^{-2}$) is the gate capacitance per unit area and is deduced from $C_0 = \epsilon\epsilon_0/h$, where ϵ (3.9 for SiO_2) and h (300 nm) are the dielectric constant and the thickness of the SiO_2 dielectric layer, respectively. From Equation (1), we note that μ_n increases with increasing doping level and a maximum value of $17.3\text{ cm}^2\text{V}^{-1}\text{s}^{-1}$ is obtained for Sample C. Although the increase of μ_n obviously departs from the conventional assumption that the mobility in a semiconductor tends to decrease at higher doping level owing to the enhanced carrier scattering,

this phenomenon is often observed for nano-FET sensors fabricated from semiconductor nanostructures. The enhanced channel conduction and the improved electrical contact at higher doping levels are considered important factors.^[20] On the other hand, electron concentration (n) is calculated according to the following relationship shown in Equation (2):

$$n = \frac{\sigma}{\mu_n q} \quad (2)$$

where σ is the NR's conductivity, and q is the elementary charge. Significantly, n increases remarkably with the increasing Cl doping and reached $6.9 \times 10^{17} \text{ cm}^{-3}$ for Sample C. This value is comparable with the previous results for n-type ZnSe films and unambiguously demonstrates that Cl could be an efficient n-type dopant for ZnSe nanostructures.^[21]

Owing to the appropriate band-gap and the high crystalline quality, ZnSe NRs have great potential as high-performance photodetectors operated at short wavelengths.^[22] Figure 4a

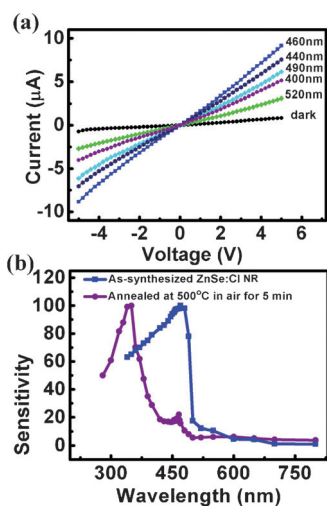


Figure 4. a) I - V curves of the ZnSe:Cl NR under light illumination with different wavelength at a constant light intensity of approximately 0.6 mW cm^{-2} . b) Spectroscopic response of the as-synthesized and annealed ZnSe:Cl NR. The voltage bias was fixed at +5 V.

plots the wavelength (λ) dependent I - V curves obtained when the ZnSe:Cl NR (Sample B) was exposed to the monochromatic light at a constant light intensity of approximately 0.60 mW cm^{-2} . It is seen that the NR's conductance strongly depends on the light wavelength, which increases with decreasing wavelength and reaches the maximum value at approximately 460 nm. Nevertheless, further shortening of the wavelength results in the decline of the conductance. Figure 4b shows the spectroscopic dependence of the sensitivity; it is found that the ZnSe:Cl NR has highest sensitivity at the blue-light region with the cut-off wavelength at approximately 490 nm, which is consistent with the band-gap of ZnSe, thus revealing that the enhancement of the photocurrent mainly originates from the electron-hole pairs excited by the incident light with energy larger than the band-gap. The decrease of the sensitivity at shorter wavelengths could be attributed to

the enhanced surface absorption and recombination. To enhance the UV response of the ZnSe:Cl NRs, the NRs were further annealed in air at 500°C for 5 minutes so as to form a thin ZnO oxide layer on the surface of the NR. As ZnO has a wider band-gap of 3.37 eV, the formation of a ZnSe/ZnO cable structure is conducive to enhance the UV response of the ZnSe NR. This assumption is confirmed by the spectroscopic response of the ZnSe:Cl NR obtained after annealing (Figure 4b), a strong response peak at approximately 350 nm corresponding to the ZnO outer shell has appeared in addition to the original ZnSe peak at approximately 460 nm, thus indicating that the spectroscopic response of the NRs in the blue to UV range could be readily controlled by this simple post-annealing process.

Figure 5 shows the time response spectra of the ZnSe NRs with varied levels of doping. All the devices exhibit excellent stability and reproducibility, however, it is also clear that the

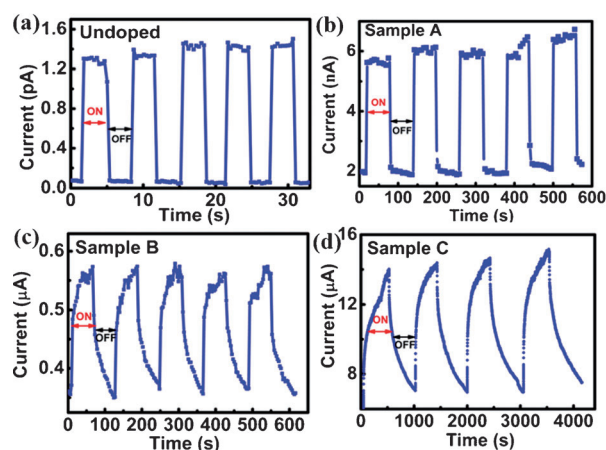


Figure 5. Time response spectra of both the undoped and chlorine-doped ZnSe NRs at fixed voltage bias of +5 V. a) undoped ZnSe NR. b) Sample A. c) Sample B. d) Sample C. The blue light (460 nm , 0.4 mW cm^{-2}) was turned ON and OFF manually.

photocurrent of the undoped ZnSe NR is much lower than that of the doped NRs. The photocurrent increases with increased doping. Responsivity (R) of a photodetector is defined in Equation (3):

$$R(\text{A/W}) = \frac{I_p}{P_{\text{opt}}} = \eta \left(\frac{q\lambda}{hc} \right) G \quad (3)$$

where I_p , P_{opt} , η , h , c , λ , and G are photocurrent, incident light power, quantum efficiency, Planck's constant, light speed, light wavelength, and photoconductive gain, respectively. Based on this equation, R is estimated to be as low as $1.4 \times 10^{-1} \text{ AW}^{-1}$ for the undoped ZnSe NR by assuming $\eta=1$ for simplify (Table 2), whereas R dramatically increases to 4.1×10^2 , 1.9×10^4 , and $7.9 \times 10^5 \text{ AW}^{-1}$ for Sample A, Sample B and Sample C, respectively. Accordingly, the photoconductive gain is enhanced from 3.7×10^{-1} for undoped NR to 1.1×10^3 for Sample A, 5.1×10^4 for Sample B, and 2.1×10^6 for Sample C. It is worth

Table 2. Key device parameters of the photodetectors based on both the undoped and chlorine-doped ZnSe NRs.				
ZnSe NRs	t_r [s]	t_f [s]	R [AW^{-1}]	G
Undoped	0.3	0.3	1.4×10^{-1}	3.7×10^{-1}
Sample A	2	2	4.1×10^2	1.1×10^3
Sample B	27.6	42.8	1.9×10^4	5.1×10^4
Sample C	120.2	394.2	7.9×10^5	2.1×10^6

noting that R and G in this study represent one of the best values obtained for the nano-photodetectors in the blue/UV range. These values are much higher than those of the commercial photodetectors fabricated from ZnSe films ($R = 0.128 \text{ AW}^{-1}$).^[23] The ZnSe:Cl NRs with such a high gain have great potential for weak light detection with detectivity even down to a single photon.^[24] The substantial improvement in R and G for the ZnSe:Cl NRs could be attributed to 1) the good Ohmic contact of ITO with the ZnSe:Cl NRs and consequently large photocurrent. 2) The high crystalline quality of the ZnSe NRs, thus giving high quantum efficiency. 3) The surface-energy-band bending near the NR surface that causes the separation of the photo-generated electron-hole pairs, i.e. holes will accumulate at the NR surface, while electrons accumulate at the bulk. As a result, the carrier lifetime is remarkably prolonged and more carriers can pass through the electrode in a certain time. 4) The Cl donors in the ZnSe NR may serve as the trapping centers for the holes, thus leading to the prolongation of the carrier lifetime. On the other hand, a longer response time is usually observed for the sample with higher doping levels (Figure 5). Both the rise time (t_r) and fall time (t_f) for the undoped NR are about 0.3 s, which in contrast to the prolonged time for Sample A (t_r 2 s, t_f 2 s), Sample B (t_r 27 s, t_f 42 s), and Sample C (t_r 120 s, t_f 394 s). It is suggested that the carrier traps induced by the Cl doping are responsible for this result. The carrier traps can capture the photo-generated carriers during the light illumination and then gradually release them after the light is OFF, thus leading to the slow response speed.

The outstanding mechanical properties of one-dimensional nanostructures such as extraordinary flexibility and resilience have attracted much attention to terms of their potential applications in flexible and transparent optoelectronics. Here, we conduct a primary study on the flexible photodetectors based on the ZnSe:Cl NRs by using PET flexible substrate instead of the rigid SiO_2/Si substrate. Figure 6a shows I - V curves of the device measured in the dark and under illumination with blue light, respectively. It is seen that the device maintains good device characteristics with linear shape I - V curves and large photocurrent. Time response spectra of the device measured at flat and under strain (0.15%) conditions are near identical, thus revealing the excellent stability of the device. Moreover, no obvious changes in dark current and photocurrent are observed as the tensile strain is applied between 0–0.35% and after the bending of 50 cycles (Figure 6c,d), further indicating that the flexible device is durable and stable within the detection range.

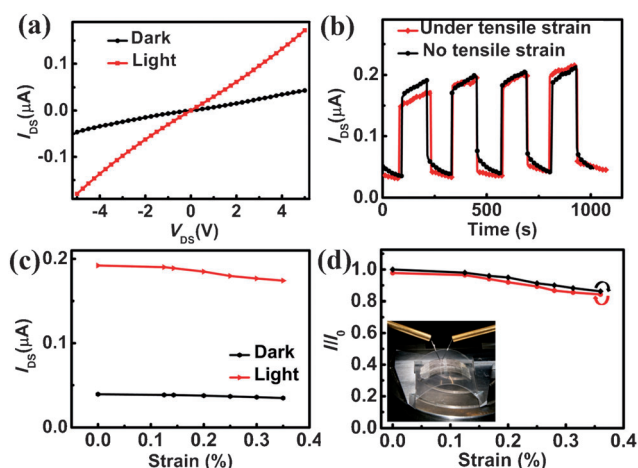


Figure 6. (a) I - V curves of the flexible ZnSe:Cl NR photodetector measured in the dark and under light illumination (460 nm , 0.4 mW cm^{-2}), respectively. The flexible PET substrate was used. (b) Time response spectra measured without tensile strain and under tensile strain of 0.15%. (c) Dark current and photocurrent measured at varied strain from 0% to 0.35%. (d) Current variation of device by applying (forwards) and removing (backwards) the strain gradually, revealing the good stability of the device. The photo in the inset shows the measurement configuration for the flexible photodetector.

Conclusions

In summary, n-type ZnSe NRs were synthesized using ZnCl_2 as the Cl dopant by an in situ doping process. The ZnSe:Cl NRs were single crystalline with wurtzite structure. The Cl doping led to the remarkable enhancement of the NR's conductivity, which could be further tuned over three orders of magnitude by varying the doping level. The field-effect transistors based on ZnSe:Cl NRs showed pronounced n-channel device characteristics with a deduced electron concentration of up to $6.9 \times 10^{17} \text{ cm}^{-3}$. Highly sensitive blue/UV light photodetectors with an extremely high photoconductive gain of 2.1×10^6 were constructed from the ZnSe:Cl NRs. Furthermore, their UV response could be improved through annealing in air. Flexible ZnSe:Cl NR photodetectors fabricated on PET substrates also exhibited excellent stability and durability. Our results demonstrate the promising applications of ZnSe:Cl NRs with tunable optoelectronic properties in new-generation nano-optoelectronic devices.

Experimental Section

Synthesis of ZnSe:Cl NRs

Chlorine-doped ZnSe NRs were synthesized in a horizontal tube furnace by a thermal co-evaporation method. Briefly, 0.3 g of ZnSe (99.99%, Aldrich) and ZnCl_2 (99.99%, Aldrich) mixed powder was loaded into an alumina boat and transferred to the center region of the furnace. The ZnCl_2 served as the Cl dopant because it could decompose at a relative low temperature. Ultrasonically cleaned Si substrates were coated with 10 nm of gold catalyst and placed downstream, i.e. approximately 10 cm away from the ZnSe/ ZnCl_2 source. The H_2 (5% in Ar) carrier gas was fed at a constant flow rate of 20 sccm and the gas pressure in the reaction chamber was

adjusted to 100 Torr. Afterwards, the mixed powder was heated up to 1020 °C in 1 h and maintained at that temperature for 2 h. A layer of bright yellow colored product could be observed on the Si substrates after growth. In this study, three samples with various Cl doping levels were synthesized. These samples were labeled as Sample A, Sample B, and Sample C, corresponding to the ZnSe/ZnCl₂ molar ratio of 8:1, 4:1, and 2:1, respectively, in the mixed powder. Undoped ZnSe NRs were synthesized under the same conditions except ZnCl₂ was not used.

Characterizations of ZnSe:Cl NRs

Morphologies and structures of the ZnSe:Cl NRs were characterized by X-ray diffraction (XRD, Rigaku D/Max-rB) with Cu_{Kα} radiation, field-emission scanning electron microscopy (FESEM, SIRION 200 FEG), and high-resolution transmission electron microscopy (HRTEM, JEOL JEM-2010). Compositions were analyzed by energy-dispersive X-ray spectroscopy (EDS, attached on the SEM) and X-ray photoelectron spectroscopy (XPS, Thermo ESCALAB 250). Room-temperature photoluminescence (RT-PL, LabRAM-HR) spectra were obtained under the excitation at 325 nm of a He-Cd laser.

Device construction and analysis

To assess the transport properties of the ZnSe:Cl NRs, back-gate field-effect transistors (FETs) based on individual ZnSe:Cl NRs were constructed. The NRs were first dispersed onto SiO₂ (300 nm)/P⁺-Si substrates with desired density, and then the indium-doped tin oxide (ITO) source and drain electrodes (120 nm) were deposited on the NRs through a pulsed laser deposition (PLD) system with KrF excimer laser (Lambda Physik COM-PexPro 102, 248 nm, 120 mJ, 5 Hz) under the assistance of a shadow mask that consisted of tungsten wires (5 μm thick). The degenerately doped Si substrate then acted as the back gate electrode. To fabricate the flexible photodetectors, PET flexible substrates instead of the rigid SiO₂/Si substrates were used and the devices were constructed by the same process described above. Electrical measurements were conducted at RT by using a semiconductor characterization system (Keithley 4200-SCS). To measure the photoconductive characteristics of the ZnSe:Cl NRs, a light source combining a xenon lamp (150 W) and a monochromator (Omni-λ.300) was used to provide the monochromatic light, which was focused and guided onto the NRs in a perpendicular manner.

Acknowledgements

This study was supported by the Major Research Plan of the National Natural Science Foundation of China (No. 91027021), the Program for New Century Excellent Talents in Universities of the Chinese Ministry of Education (No. NCET-08-0764), and the National Natural Science Foundation of China (NSFC; Nos. 60806028, 51172151, 20901021, 21101051, and 61106010).

Keywords: doping · field-effect transistors · nanostructures · photodetectors · ZnSe nanoribbons

- [1] M. Benedicto, B. Galiana, J. M. Molina-Aldareguia, S. Monaghan, P. K. Hurlley, K. Cherkaoui, L. Vazquez, P. Tejedor, *Nanoscale Res. Lett.* **2011**, *6*, 400–406.
- [2] S. Jha, J. C. Qian, O. Kutsay, J. Kovac, Jr., C. Y. Luan, J. A. Zapien, W. J. Zhang, S. T. Lee, I. Bello, *Nanotechnology* **2011**, *22*, 245202–245210.
- [3] F. Grosshans, G. Van Assche, J. Wenger, R. Brouri, N. J. Cerf, P. Grangier, *Nature* **2003**, *421*, 238–241.
- [4] W.-C. Kwak, S.-H. Han, T. G. Kim, Y.-M. Sung, *Cryst. Growth Des.* **2010**, *10*, 5297–5301.
- [5] Y. Jiang, X. M. Meng, W. C. Yiu, J. Liu, J. X. Ding, C. S. Lee, S. T. Lee, *J. Phys. Chem. B* **2004**, *108*, 2784–2787.
- [6] T. L. Spencer, R. Cisek, V. Barzda, U. Philipose, H. E. Ruda, A. Shik, *Appl. Phys. Lett.* **2009**, *94*, 233119–233122.
- [7] J. Basu, R. Divakar, J. Nowak, S. Hofmann, A. Colli, A. Franciosi, C. B. Carter, *J. Appl. Phys.* **2008**, *104*, 064302–064310.
- [8] P. T. K. Chin, J. W. Stouwdam, R. A. J. Janssen, *Nano Lett.* **2009**, *9*, 745–750.
- [9] X. T. Zhang, K. M. Ip, Q. Li, S. K. Hark, *Appl. Phys. Lett.* **2005**, *86*, 203114–203117.
- [10] B. J. Xi, D. C. Xu, S. L. Xiong, C. M. Wang, X. M. Feng, H. Y. Zhou, Y. T. Qian, *J. Phys. Chem. C* **2008**, *112*, 5333–5338.
- [11] E. Tournié, C. Morhain, G. Neu, J. P. Faurie, *Phys. Rev. B* **1997**, *56*, R1657–R1660.
- [12] X. W. Zhang, J. S. Jie, Z. Wang, C. Y. Wu, L. Wang, Q. Peng, Y. Q. Yu, P. Jiang, C. Xie, *J. Mater. Chem.* **2011**, *21*, 6736–6741.
- [13] Q. Peng, J. S. Jie, C. Xie, L. Wang, X. W. Zhang, D. Wu, Y. Q. Yu, C. Y. Wu, Z. Wang, P. Jiang, *Appl. Phys. Lett.* **2011**, *98*, 123117–123120.
- [14] D. Wu, Y. Jiang, S. Y. Li, F. Z. Li, J. W. Li, X. Z. Lan, Y. G. Zhang, C. Y. Wu, L. B. Luo, J. S. Jie, *Nanotechnology* **2011**, *22*, 405201–405206.
- [15] C. X. Shan, Z. Liu, X. T. Zhang, C. C. Wong, S. K. Hark, *Nanotechnology* **2006**, *17*, 5561–5564.
- [16] U. Philipose, H. E. Ruda, A. Shik, C. F. de Souza, P. Sun, *J. Appl. Phys.* **2006**, *99*, 066106–066109.
- [17] H. Wang, T. Tian, S. Yan, N. Huang, Z. Xiao, *J. Cryst. Growth* **2009**, *311*, 3787–3791.
- [18] A. E. Martínez-Cantón, M. García-Rocha, I. Hernández-Calderon, R. Ortega-Martínez, *Microelectron. J.* **2005**, *36*, 527–530.
- [19] J. S. Wang, W. J. Chen, C. S. Yang, Y. H. Tsai, H. H. Wang, R. H. Chen, J. L. Shen, C. D. Tsai, *Appl. Phys. Lett.* **2011**, *98*, 021908–021911.
- [20] G. F. Zheng, W. Lu, S. Jin, C. M. Lieber, *Adv. Mater.* **2004**, *16*, 1890–1893.
- [21] G. Karczewski, B. Hu, A. Yin, H. Luo, J. K. Furdyna, *J. Appl. Phys.* **1994**, *75*, 7382–7388.
- [22] X. S. Fang, S. L. Xiong, T. Y. Zhai, Y. Bando, M. Y. Liao, U. K. Gautam, Y. Koide, X. G. Zhang, Y. T. Qian, D. Golberg, *Adv. Mater.* **2009**, *21*, 5016–5021.
- [23] T. K. Lin, S. J. Chang, Y. K. Su, Y. Z. Chiou, C. K. Wang, S. P. Chang, C. M. Chang, J. J. Tang, B. R. Huang, *Mater. Sci. Eng. B* **2005**, *119*, 202–205.
- [24] Y. Q. Yu, J. S. Jie, P. Jiang, L. Wang, C. Y. Wu, Q. Peng, X. W. Zhang, Z. Wang, C. Xie, Y. Jiang, *J. Mater. Chem.* **2011**, *21*, 12632–12639.

Received: November 29, 2011

Published online on April 12, 2012